(Review)

Development of HANABI, an ultrasonication-forced amyloid fibril inducer

Yuji Goto[a,*] Kichitaro Nakajima[a], Keiichi Yamaguchi[a], Masatomo So[b], Kensuke Ikenaka[c], Hideki Mochizuki[c], and Hirotsugu Ogi[d]

[a]Global Center for Medical Engineering and Informatics, Osaka University, 2-1 Yamadaoka, Suita, Osaka 565-0871, Japan

[b]Institute for Protein Research, Osaka University, 3-2 Yamadaoka, Suita, Osaka 565-0871, Japan

[c]Department of Neurology, Graduate School of Medicine, Osaka University, 2-2 Yamadaoka, Suita, Osaka 565-0871, Japan

[d]Graduate School of Engineering, Osaka University, Suita, Osaka 565-0871, Japan

*Corresponding author: Yuji Goto

E–mail: gtyj8126@protein.osaka-u.ac.jp; Phone: +81-6-6879-4100.

Abstract: Amyloid fibrils involved in amyloidoses are crystal-like aggregates, which are formed by breaking supersaturation of denatured proteins. Ultrasonication is an efficient method of agitation for breaking supersaturation and thus inducing amyloid fibrils. By combining an ultrasonicator and a microplate reader, we developed the HANABI (HANdai Amyloid Burst Inducer) system that enables high-throughput analysis of amyloid fibril formation. Among high-throughput approaches of amyloid fibril assays, the HANABI system has advantages in accelerating and detecting spontaneous amyloid fibril formation. HANABI is also powerful for amplifying a tiny amount of preformed amyloid fibrils by seeding. Thus, HANABI will contribute to creating therapeutic strategies against amyloidoses by identifying their biomarkers.

Keywords: α-synuclein; β_2-microglobulin; amyloid fibril; solubility; supersaturation; ultrasonication

1. Supersaturation-dependent amyloid fibril formation

Soon after the discovery of prion phenomena including kuru and scrapie diseases, even without knowledge of the responsible agent, it was recognized that prion disease transmission and propagation shared commonalities with the process of crystallization (Griffith, 1967; So et al., 2016). Crystallization of a solute occurs when the solute concentration is higher than its thermodynamic solubility (i.e., supersaturation) upon breaking supersaturation (Fig. 1) (Coquerel, 2014). In general, supersaturation is required for formation of crystals and crystal-like structures of solutes. Moreover, the supersaturation phenomenon is common in temperature-dependent liquid-solid or vapor-liquid phase transitions of substances, with one well-known example being the super-cooling of water prior to ice formation. However, physicochemical mechanisms underlying supersaturation remain elusive (Coquerel, 2014; Matsushita et al., 2015; Matsushita et al., 2017; Wallace et al., 2013).

Subsequent studies exploring the structural and functional relationships between amyloid fibrils and amyloidoses including prion diseases established this paradigm: Amyloid fibril formation is "one-dimensional crystallization": (Jarrett and Lansbury, 1993; So et al., 2016; Wetzel, 2006). The key pieces of evidence supporting this linkage were that: (i) spontaneous amyloid fibril formation occurs by a nucleation and growth mechanism, requiring a long lag time, (ii) seeding (seed-dependent propagation) is an efficient approach for accelerating amyloid fibril formation by escaping the high energy barrier associated with spontaneous nucleation, and (iii) amorphous aggregates predominate under solute conditions well above the solubility.

Investigations into the temporal evolution of major biomarkers of Alzheimer's disease (Bateman et al., 2012; Jack et al., 2013) in the onset and progression of clinical symptoms has provided important insights into the role of supersaturation, a required condition for both crystal formation and amyloid fibril formation. Most importantly, concentrations of amyloid β(1-42)

peptide (Aβ(1-42)) in the cerebrospinal fluid (CSF) decline 25 and 15 years before expected symptom onset and Aβ(1-42) deposition, respectively. Similar decreases in the α-synuclein (aSN) concentration were reported for Parkinson's disease (Hong et al., 2010; Kang et al., 2013; Mollenhauer et al., 2011; Parnetti et al., 2019; Tokuda et al., 2006). Here the supersaturation hypothesis provides a simple physical explanation as to why the CSF Aβ(1-42) or aSN decreases concomitantly with the deposition of amyloid fibrils (Guo, 2021; So et al., 2016). The increase in the Aβ(1–40)/Aβ(1–42) ratio for plasma of individuals with Alzheimer's disease (Nakamura et al., 2018) might be also explained by the supersaturation hypothesis: Breakdown of supersaturation decreases the soluble concentration of Aβ(1-42) more than that of Aβ(1-40).

2. Ultrasonication-dependent amyloid fibril formation

2.1. Amplification of preformed amyloid fibrils

Based on basic properties of amyloid fibril formation, seeding has been routinely used to propagate amyloid fibrils. Ultrasonication treatments are useful for seeding experiments by increasing the number of active seeds (Table 1). For the reproduction of various types of amyloid fibrils, e.g., β2-microglobulin (β2m) and amyloid β peptide (Aβ) associated with dialysis-related amyloidosis and Alzheimer's disease, respectively, Naiki and coworkers used an ultrasonic disruptor to fragment the amyloid fibrils purified from patients (Naiki and Gejyo, 1999; Naiki et al., 1998; Naiki et al., 1997). It was shown later that extensive ultrasonication maximally fragments the preformed amyloid fibrils of β2m, producing monodispersed amyloid fibrils of minimal size (amyloid particles) with an average molecular weight of 1,660,000 (140-mer) (Chatani et al., 2009; Yoshimura et al., 2010).

Ultrasonication was also used for Protein Misfolding Cyclic Amplification (PMCA), an important methodology for detecting seed-competent prion aggregates in patients (Saborio et al.,

2001) (Table 1). It has been suggested that, during the time between infection and appearance of clinical symptoms, minute amounts of disease-associated prion (PrP^{Sc}) replicate by conformational conversion of host normal cell-surface prion (PrP^{C}), generating large amounts of $PrPS^{Sc}$ aggregates in the brains of diseased individuals (Paciotti et al., 2018; Saborio et al., 2001). Ultrasonication-dependent PMCA can reproduce this event in vitro by repeating the fragmentation of infectious aggregates and amplification by seeding. Today, it is considered that PrP^{C} and PrP^{SC} correspond to monomers and amyloid-like aggregates, respectively, of the same prion protein. PMCA has been applied successfully to detect the presence of infectious agents in tissues and biological fluids and, moreover, to diagnose prion diseases (Concha-Marambio et al., 2016) and α-synucleopathies (Becker et al., 2018; Fenyi et al., 2019; Shahnawaz et al., 2020). When PMCA was introduced around 2000, spontaneous amyloid fibril formation was not expected to occur by ultrasonication and the PMCA methodology was aimed at amplifying preformed amyloid-like aggregates by a mechanism conceptually analogous to polymerase chain reaction cycling.

In a similar fashion, Real-Time Quaking-Induced Conversion (RT-QuIC) was developed (Table 1), where the amplification of prion seeds in microplate wells was performed by shaking (Atarashi et al., 2011; Orru et al., 2015; Paciotti et al., 2018). RT-QUIC was also successfully applied for α-synucleopathies (Fairfoul et al., 2016; Sano et al., 2018).

2.2. Ultrasonication-triggered spontaneous amyloid fibril formation

Crystallization of a solute under supersaturation can be triggered by various types of agitation. In other words, agitations have the potential to trigger amyloid nucleus formation. In fact, shaking or stirring of solution has been used widely to promote the formation of amyloid fibrils (Giehm and Otzen, 2010; Kad et al., 2003) (Table 1). While acid-unfolded β2m under quiescence

cannot form amyloid fibrils at pH 2.5 without seeding, vigorous stirring of the sample solution induced mature amyloid fibrils even in the absence of seeds (Kad et al., 2003).

Ultrasonication, conventionally used for preparing seed amyloid fibrils, is another type of agitation that might trigger the nucleation process. Stathopulos et al. (Stathopulos et al., 2004) first reported that, for various proteins, ultrasonication resulted in the formation of amyloid-like aggregates. They suggested that protein unfolding and aggregation are caused by ultrasonication, leading to the formation of amyloid fibrils.

Ohhashi et al. (Ohhashi et al., 2005) examined the effects of ultrasonication on β2m at pH 2.5. The ultrasonicator used was a water bath-type model with incident beams of ultrasonication (near 19 kHz) from three directions focused near the surface of the water bath (Fig. 2A). Samples in Eppendorf tubes were placed near the surface to receive maximal ultrasonication. Upon ultrasonic irradiation of an acid-unfolded β2m solution at pH 2.5, thioflavin T (ThT) fluorescence increased markedly after a lag time of 1–2 h with a simultaneous increase of light scattering. Atomic force microscopy (AFM) images showed the formation of a large number of short fibrils 3 nm in diameter. When the sonication-induced amyloid fibrils were used as seeds in the next seeding experiment, rapid and intense formation of long amyloid fibrils 3 nm in diameter was observed, demonstrating seed-dependent amyloid fibril growth.

So et al. (So et al., 2011) combined the use of an ultrasonicator and a microplate reader as a high-throughput approach to studying the potential of proteins to form amyloid fibrils. In a standard experiment, the 96 wells were filled with sample solutions of β2m (0.2 mL each at 0.3 mg/mL and pH 2.5) containing 5 μM ThT (Fig. 2). The plate was ultrasonicated with various sequences of irradiation pulses (cycles of 1-min ultrasonication followed by 9-min quiescence).

After ultrasonication treatment, the plate was set on the microplate reader to assay ThT fluorescence. The process was repeated during the incubation period.

The results were consistent with those obtained with Eppendorf tubes (Ohhashi et al., 2005). However, as anticipated from the relatively wide microplate used (6 x 10 cm with 8 x 12 wells), the lag-time for fibril formation (t_{lag}) varied significantly depending on the location in the microplate, and the final fluorescence intensity also varied. Generally, the wells located in the center of the plate tended to show a shorter lag time and these locations were consistent with positions most likely to receive ultrasonic waves. To minimize the difference depending on the well position, the microplate was rotated horizontally at the center with a special holder. Upon rotation of the microplate, synchronization of amyloid fibril formation occurred as well as slight shortening of the lag time.

3. HANdai Amyloid Burst Inducer (HANABI)

3.1. Design and basic performance

Umemoto et al. (Umemoto et al., 2014) then constructed the instrument HANABI which combines a water bath-type ultrasonicator and microplate reader (Fig. 3). With the HANABI system, ultrasonic irradiation was performed in a water bath, the plate was then moved to the microplate reader, and ThT fluorescence was monitored; these three processes were repeated automatically based on programmed time schedules. Moreover, the plate was moved along x-y axes in sequence to ultrasonicate the 96 wells evenly. A typical movement was 5 cm along the x axis, 10 cm along the y axis, -5 cm along the x axis, and -10 cm along the y axis in sequence.

To assess the performance of the HANABI system, Umemoto et al. (Umemoto et al., 2014) examined the standard amyloid fibril formation of β2m (0.3 mg/mL β2m in 100 mM NaCl at pH 2.5) in 96-well plates with cycles of 1 min of ultrasonication and 9 min of quiescence (Fig. 4). In

the absence of plate movements, the lag time varied significantly from 1.5 to 10 h depending on the wells. In contrast, plate movements led to synchronized amyloid fibril formation with a lag time of 1–1.5 h. The extent of variation among the 96 wells was analyzed on the basis of the lag time in the presence or absence of plate movements. In the absence of plate movements, the mean ± S.D. and coefficient of variation (CV) were 6.0 ±4.0 h and 0.85, respectively. In the presence of plate movements, the amyloid burst synchronized with a mean ± S.D. and CV of 2.0 ± 0.4 h and 0.2, respectively.

3.2. Detection of α-synuclein aggregates in cerebrospinal fluid

Kakuda et al. (Kakuda et al., 2019) used the HANABI system to amplify and detect α-synuclein aggregates with seeding activity from CSF, and investigated the correlation between seeding activity and clinical indicators. The seeding activity of CSF correlated with the levels of αSN oligomers measured by an enzyme-linked immunosorbent assay. Moreover, the seeding activity of CSF from patients with Parkinson's disease was higher than that of control patients. Notably, the lag time of patients with Parkinson's disease was significantly correlated with the ^{123}I-meta-iodobenzylguanidine (MIBG) heart-to-mediastinum (H/M) ratio, one of the most specific radiological features of Parkinson's diseases and dementia with Lewy bodies. These findings showed that the HANABI assay can evaluate the seeding activity of CSF by amplifying misfolded α-synuclein aggregates.

3.3. Ultrasonication-dependent crystallization of lysozyme

Ultrasonication was previously shown to be useful for accelerating the crystallization of proteins (Crespo et al., 2010; Kitayama et al., 2013). Umemoto et al. (Umemoto et al., 2014) installed a CCD camera in the HANABI system to rapidly and automatically monitor the crystallization of hen egg white lysozyme solution at a concentration of 20 mg/mL at pH 4.8 and

25 °C (Fig. 5). No crystals were observed after 1 day of incubation at 1.0 M NaCl in the absence of agitation (Fig. 5A). However, when the solution was subjected to ultrasonication for 5 min, crystals appeared at 10 h and grew in size by 30 h (Fig. 5B) – 50 h (Fig. 5D). Extensive ultrasonication, which was achieved by repeated pulses, resulted in a large number of small and homogeneous crystals (Fig. 5C). These results indicated that ultrasonic irradiation broke supersaturation, leading to protein crystallization.

3.4. Optimized sonoreactor for accelerative amyloid-fibril assays

Although the original HANABI system promoted ultrasonication efficacy, several challenges remained. In general, acoustic field in a sample solution could not be the same because of changes in temperature, the volume of the water, and the distribution of the dissolved gases in the water bath. In particular, for the amyloid-fibril assay, a long-time ultrasonication over tens of hours leads to significant changes in the water bath conditions, deteriorating the reproducibility of the acoustic field that directly affects the fibril-formation reaction. Furthermore, in the original HANABI system, the fluorescence signal was acquired from the upper surface of the microplate, which was significantly affected by water droplets on the microplate because of the high-power ultrasonication.

Nakajima et al. (Nakajima et al., 2021a) developed a HANABI-2000 system with an optimized sonoreactor for the amyloid-fibril assay, which improved the reproducibility and controllability of the amyloid fibril formation (Fig. 6). First, the water bath was eliminated in order to conduct a reproducible analysis. A single rod-shaped ultrasonic transducer was placed on each sample solution in an assay plate. The resonant frequency of the transducer was 30 kHz, which is optimized for accelerating fibril formation (Nakajima et al., 2016). Second, a microphone was placed below the assay plate to measure the acoustic intensity of each sample solution. The acoustic-intensity measurement allows to control the acoustic field in each well by individually

controlling the voltage and frequency of the driving signal applied to each transducer. Third, a photodetector was placed beneath the microplate to measure the fluorescent signal, which improves the signal-to-noise ratio of the fluorescence measurement because of the absence of the water bath.

Using β2m, Nakajima et al. (Nakajima et al., 2021a) demonstrated that achieving identical acoustic conditions by controlling the oscillation amplitude and frequency of each transducer results in synchronized amyloid fibril formation behavior across 36 solutions. They then succeeded in detecting 100-fM seeds at an accelerated rate. Moreover, they revealed that acceleration of the amyloid fibril formation reaction with the seeds is achieved by enhancing the primary nucleation and fibril fragmentation. These results suggested the efficacy of HANABI-2000 for the diagnosis of amyloidosis owing to the accelerative seed detection and possibility for further early-stage diagnosis even without seeds through the accelerated primary nucleation (i.e., identification of susceptibility risk biomarker (Parnetti et al., 2019)).

4. Underlying mechanisms of ultrasoniciation-dependent amyloid formation

4.1. Cavitation-bubble dynamics

Ultrasonic waves (i.e., 20–300 kHz) develop compression and rarefaction while transmitting through the medium. Cavitation bubbles are generated by negative pressure of driving ultrasonic wave (Fig. 7). They could stably oscillate in case of low acoustic pressures, but show the transient cavitation behavior under high pressures, where bubbles grow relatively slowly and collapse rapidly, causing extremely high temperature region near the bubbles, called hot spots. The hot spot temperature exceeds 10,000 K (Nakajima et al., 2016).

Nakajima et al. (Nakajima et al., 2016) studied the molecular mechanism underlying the ultrasonication-dependent acceleration of amyloid fibril formation. They showed that ultrasonic cavitation bubbles behave as catalysts for nucleation: The nucleation reaction was highly dependent

on the frequency and pressure of acoustic waves and, under optimal acoustic conditions, the reaction-rate constant for nucleation increased by three orders of magnitude. A theoretical model was proposed to explain the markedly frequency- and pressure-dependent nucleation, where monomers are captured on the bubble surface during its growth and highly condensed by subsequent bubble collapse, so that they are transiently exposed to high temperatures (Fig. 7). Thus, the dual effects of local condensation and local heating contribute to markedly enhancing the nucleation reaction. Their model consistently reproduced the frequency and pressure dependences, supporting its essential applicability.

4.2. Comparison of ultrasonication and shaking

Although both ultrasonication and shaking are effectively used to induce amyloid fibril formation and propagation (Table 1), the difference between them remained unclear. Nakajima et al. (Nakajima et al., 2021b) comprehensively compared ultrasonication and shaking with respect to the morphology and structure of resultant β2m aggregates, kinetics of amyloid fibril formation, and seed-detection sensitivity. They focused on a half-time (t_{half}), a time required for exhibiting a half of the maximal ThT fluorescence and constructed heat map, which describes the phase diagram of β2m aggregation. The experimental results showed that ultrasonication markedly promotes amyloid fibril formation, especially in dilute monomer solutions, induces short-dispersed fibrils, and is capable of detecting ultra-trace-concentration seeds with a detection limit of 10 fM.

Most importantly, they indicated that ultrasonication highly alters the energy landscape of an aggregation reaction due to the effect of ultrasonic cavitation. Under shaking (Fig. 8B), the metastable region becomes narrower than that under quiescence (Fig. 8A), showing that shaking induces a downward shift of the metastable−labile boundary, whereas the labile−amorphous boundary is little affected. On the other hand, ultrasonication causes not only a significant

downward shift of the metastable−labile boundary but also an upward shift of the labile−amorphous boundary (Fig. 8C).

In the labile region, although the acceleration ability of shaking was similar to that of ultrasonication for solutions with high monomer concentrations, it deteriorated for solutions with a monomer concentration lower than 0.1 mg/mL. The aggregation acceleration by shaking results from the increase in the apparent mean-free path of monomer movements. Thus, shaking enhances the probability of intermolecular interactions in a condensed solution by increasing the collision frequency among monomers. However, it fails to increase the collision frequency in a dilute solution, diminishing the acceleration effect for nucleation (Fig. 8B). In contrast, ultrasonication retains high acceleration ability even for dilute monomer solutions because the cavitation bubble works as a catalyst for the nucleation reaction (Fig. 7)(Nakajima et al., 2016). On the other hand, if the bubble surface becomes fully covered with monomers, the acceleration effect saturates. This mechanism consistently explains why the t_{half} value of the ultrasonication-dependent acceleration cannot be decreased below the lower limit of ~10 h for solutions with high monomer concentrations.

5. Conclusions

A useful literary analogy describing the similarities between amyloid fibril formation and crystallization has been suggested on the basis of Kurt Vonnegut's novel "Cat's Cradle" (Lansbury and Caughey, 1995; Vonnegut, 1963). In this fictional work, ice 9, a high temperature ice nucleus (stable at 45.8°C) was created to help troops escape from mud; however, it turned out to be an Armageddon device: once a small block of ice 9 was exposed to water, it started a world-wide water 'freeze' due to seed-dependent propagation. Although the similarity between amyloid fibril formation and crystallization was shown to be a useful paradigm at the start of amyloid research, the majority of subsequent studies have focused on the role of the aggregate structure and potential

biochemical interactions. An increasing number of atomic structures of amyloid fibrils have been reported based on the solid-state NMR and cryoEM methodologies (Sawaya et al., 2021). However, it will be difficult to understand supersaturation by structural studies. Thus, it will be increasingly important to study amyloid fibril formation on the basis of solubility and supersaturation, to which HANABI will contribute significantly. Advantages of ultrasonication are simplicity and no need to add stirrer tips. Although the effects have analogies to stirring or shaking, ultrasonication promotes amorphous aggregates less than stirring or shaking. The HANABI system can be easily combined with various additives and solvent conditions to increase specificity and sensitivity (Table 1). Technical advances in controlling supersaturation-limited phase transition will further expand the applicability of HANABI.

Finally, early diagnosis is one of the most important therapeutic strategies against neurodegenerative diseases. Thus, the need to establish diagnostic biomarkers is urgent in the field of neurodegeneration (Parnetti et al., 2019). HANABI is one of the most promising methodologies as well as PMCA and RT-QuIC (Parnetti et al., 2019). Most importantly, HANABI, originally developed for accelerating spontaneous amyloid fibril formation, will be powerful for identifying "susceptibility risk biomarkers (Parnetti et al., 2019)", i.e., the potential for an individual to develop a disease in the absence of any clinically apparent disease or medical condition.

Declaration of competing interests

The authors declare that there are no conflicts of interest.

Authors' contributions

All authors contributed to the design of the article based on their collaborative research. YG wrote the draft which was reviewed by all authors. All authors approved the final manuscript.

Acknowledgments

We thank Corona Electric Co. for technical support. This study was performed as part of the Cooperative Research Program for the Institute for Protein Research, Osaka University (CR-20-02). This study was supported by the Japan Society for the Promotion of Science (20K22484), Core-to-Core Program A (Advance Research Networks), Ministry of Education, Culture, Sports, Science and Technology (17H06352), and SENTAN from AMED (16809242).

References

Abdolvahabi, A., Shi, Y., Rasouli, S., Croom, C.M., Chuprin, A., Shaw, B.F., 2017. How do gyrating beads accelerate amyloid fibrillization? Biophys. J. 112, 250-264.

Adachi, M., So, M., Sakurai, K., Kardos, J., Goto, Y., 2015. Supersaturation-limited and unlimited phase transitions compete to produce the pathway complexity in amyloid fibrillation. J. Biol. Chem. 290, 18134-18145.

Atarashi, R., Satoh, K., Sano, K., Fuse, T., Yamaguchi, N., Ishibashi, D., Matsubara, T., Nakagaki, T., Yamanaka, H., Shirabe, S., Yamada, M., Mizusawa, H., Kitamoto, T., Klug, G., McGlade, A., Collins, S.J., Nishida, N., 2011. Ultrasensitive human prion detection in cerebrospinal fluid by real-time quaking-induced conversion. Nat. Med. 17, 175-178.

Bateman, R.J., Xiong, C., Benzinger, T.L., Fagan, A.M., Goate, A., Fox, N.C., Marcus, D.S., Cairns, N.J., Xie, X., Blazey, T.M., Holtzman, D.M., Santacruz, A., Buckles, V., Oliver, A., Moulder, K., Aisen, P.S., Ghetti, B., Klunk, W.E., McDade, E., Martins, R.N., Masters, C.L., Mayeux, R., Ringman, J.M., Rossor, M.N., Schofield, P.R., Sperling, R.A., Salloway, S., Morris, J.C., 2012. Clinical and biomarker changes in dominantly inherited Alzheimer's disease. N. Engl. J. Med. 367, 795-804.

Becker, K., Wang, X., Vander Stel, K., Chu, Y., Kordower, J., Ma, J., 2018. Detecting a synuclein seeding activity in formaldehyde-fixed MSA patient tissue by PMCA. Mol Neurobiol 55, 8728-8737.

Chatani, E., Lee, Y.H., Yagi, H., Yoshimura, Y., Naiki, H., Goto, Y., 2009. Ultrasonication-dependent production and breakdown lead to minimum-sized amyloid fibrils. Proc. Natl. Acad. Sci. U. S. A. 106, 11119-11124.

Concha-Marambio, L., Pritzkow, S., Moda, F., Tagliavini, F., Ironside, J.W., Schulz, P.E., Soto, C., 2016. Detection of prions in blood from patients with variant Creutzfeldt-Jakob disease. Sci. Transl. Med. 8, 370ra183.

Coquerel, G., 2014. Crystallization of molecular systems from solution: phase diagrams, supersaturation and other basic concepts. Chem. Soc. Rev. 43, 2286-2300.

Crespo, R., Martins, P.M., Gales, L., Rocha, F., Damas, A.M., 2010. Potential use of ultrasound to promote protein crystallization. J. Appl. Cryst. 43, 1419-1425.

Fairfoul, G., McGuire, L.I., Pal, S., Ironside, J.W., Neumann, J., Christie, S., Joachim, C., Esiri, M., Evetts, S.G., Rolinski, M., Baig, F., Ruffmann, C., Wade-Martins, R., Hu, M.T., Parkkinen, L., Green, A.J., 2016. Alpha-synuclein RT-QuIC in the CSF of patients with alpha-synucleinopathies. Ann. Clin. Transl. Neurol. 3, 812-818.

Fenyi, A., Leclair-Visonneau, L., Clairembault, T., Coron, E., Neunlist, M., Melki, R., Derkinderen, P., Bousset, L., 2019. Detection of alpha-synuclein aggregates in gastrointestinal biopsies by protein misfolding cyclic amplification. Neurobiol. Dis. 129, 38-43.

Furukawa, K., Aguirre, C., So, M., Sasahara, K., Miyanoiri, Y., Sakurai, K., Yamaguchi, K., Ikenaka, K., Mochizuki, H., Kardos, J., Kawata, Y., Goto, Y., 2020. Isoelectric point-amyloid formation of alpha-synuclein extends the generality of the solubility and supersaturation-limited mechanism. Curr. Res. Struct. Biol. 2, 35-44.

Giehm, L., Otzen, D.E., 2010. Strategies to increase the reproducibility of protein fibrillization in plate reader assays. Anal. Biochem. 400, 270-281.

Goto, Y., Adachi, M., Muta, H., So, M., 2018. Salt-induced formations of partially folded intermediates and amyloid fibrils suggests a common underlying mechanism. Biophys. Rev. 10, 493-502.

Griffith, J.S., 1967. Self-replication and scrapie. Nature 215, 1043-1044.

Guo, Z., 2021. Amyloid hypothesis through the lens of Abeta supersaturation. Neural. Regen. Res. 16, 1562-1563.

Hong, Z., Shi, M., Chung, K.A., Quinn, J.F., Peskind, E.R., Galasko, D., Jankovic, J., Zabetian, C.P., Leverenz, J.B., Baird, G., Montine, T.J., Hancock, A.M., Hwang, H., Pan, C., Bradner, J., Kang, U.J., Jensen, P.H., Zhang, J., 2010. DJ-1 and alpha-synuclein in human cerebrospinal fluid as biomarkers of Parkinson's disease. Brain 133, 713-726.

Jack, C.R., Jr., Knopman, D.S., Jagust, W.J., Petersen, R.C., Weiner, M.W., Aisen, P.S., Shaw, L.M., Vemuri, P., Wiste, H.J., Weigand, S.D., Lesnick, T.G., Pankratz, V.S., Donohue, M.C., Trojanowski, J.Q., 2013. Tracking pathophysiological processes in Alzheimer's disease: an updated hypothetical model of dynamic biomarkers. Lancet Neurol. 12, 207-216.

Jarrett, J.T., Lansbury, P.T., Jr., 1993. Seeding "one-dimensional crystallization" of amyloid: a pathogenic mechanism in Alzheimer's disease and scrapie? Cell 73, 1055-1058.

Kad, N.M., Myers, S.L., Smith, D.P., Smith, D.A., Radford, S.E., Thomson, N.H., 2003. Hierarchical assembly of beta2-microglobulin amyloid in vitro revealed by atomic force microscopy. J. Mol. Biol. 330, 785-797.

Kakuda, K., Ikenaka, K., Araki, K., So, M., Aguirre, C., Kajiyama, Y., Konaka, K., Noi, K., Baba, K., Tsuda, H., Nagano, S., Ohmichi, T., Nagai, Y., Tokuda, T., El-Agnaf, O.M.A., Ogi, H., Goto, Y., Mochizuki, H., 2019. Ultrasonication-based rapid amplification of alpha-synuclein aggregates in cerebrospinal fluid. Sci. Rep. 9, 6001.

Kang, J.H., Irwin, D.J., Chen-Plotkin, A.S., Siderowf, A., Caspell, C., Coffey, C.S., Waligorska, T., Taylor, P., Pan, S., Frasier, M., Marek, K., Kieburtz, K., Jennings, D., Simuni, T., Tanner, C.M., Singleton, A., Toga, A.W., Chowdhury, S., Mollenhauer, B., Trojanowski, J.Q., Shaw, L.M., 2013. Association of cerebrospinal fluid beta-amyloid 1-42, T-tau, P-tau181, and

alpha-synuclein levels with clinical features of drug-naive patients with early Parkinson disease. JAMA Neurol. 70, 1277-1287.

Kitayama, H., Yoshimura, Y., So, M., Sakurai, K., Yagi, H., Goto, Y., 2013. A common mechanism underlying amyloid fibrillation and protein crystallization revealed by the effects of ultrasonication. Biochim. Biophys. Acta 1834, 2640-2646.

Lansbury, P.T., Jr., Caughey, B., 1995. The chemistry of scrapie infection: implications of the 'ice 9' metaphor. Chem. Biol. 2, 1-5.

Linse, S., Cabaleiro-Lago, C., Xue, W.F., Lynch, I., Lindman, S., Thulin, E., Radford, S.E., Dawson, K.A., 2007. Nucleation of protein fibrillation by nanoparticles. Proc. Natl. Acad. Sci. U. S. A. 104, 8691-8696.

Matsushita, Y., Sekiguchi, H., Ichiyanagi, K., Ohta, N., Ikezaki, K., Goto, Y., Sasaki, Y.C., 2015. Time-resolved X-ray tracking of expansion and compression dynamics in supersaturating ion-networks. Sci Rep 5, 17647.

Matsushita, Y., Sekiguchi, H., Wong, C.J., Nishijima, M., Ikezaki, K., Hamada, D., Goto, Y., Sasaki, Y.C., 2017. Nanoscale dynamics of protein assembly networks in supersaturated solutions. Sci. Rep. 7, 13883.

Mollenhauer, B., Locascio, J.J., Schulz-Schaeffer, W., Sixel-Doring, F., Trenkwalder, C., Schlossmacher, M.G., 2011. alpha-Synuclein and tau concentrations in cerebrospinal fluid of patients presenting with parkinsonism: a cohort study. Lancet Neurol. 10, 230-240.

Morales, R., Duran-Aniotz, C., Diaz-Espinoza, R., Camacho, M.V., Soto, C., 2012. Protein misfolding cyclic amplification of infectious prions. Nat. Protoc. 7, 1397-1409.

Muta, H., Lee, Y.H., Kardos, J., Lin, Y., Yagi, H., Goto, Y., 2014. Supersaturation-limited amyloid fibrillation of insulin revealed by ultrasonication. J. Biol. Chem. 289, 18228-18238.

Naiki, H., Gejyo, F., 1999. Kinetic analysis of amyloid fibril formation. Methods Enzymol. 309, 305-318.

Naiki, H., Hasegawa, K., Yamaguchi, I., Nakamura, H., Gejyo, F., Nakakuki, K., 1998. Apolipoprotein E and antioxidants have different mechanisms of inhibiting Alzheimer's beta-amyloid fibril formation in vitro. Biochemistry 37, 17882-17889.

Naiki, H., Hashimoto, N., Suzuki, S., Kimura, H., Nakakuki, K., Gejyo, F., 1997. Establishment of a kinetic model of dialysis-related amyloid fibril extension in vitro. Amyloid 4, 223-232.

Nakajima, K., Noi, K., Yamaguchi, K., So, M., Ikenaka, K., Mochizuki, H., Ogi, H., Goto, Y., 2021a. Optimized sonoreactor for accelerative amyloid-fibril assays through enhancement of primary nucleation and fragmentation. Ultrason. Sonochem. 73, 105508.

Nakajima, K., Ogi, H., Adachi, K., Noi, K., Hirao, M., Yagi, H., Goto, Y., 2016. Nucleus factory on cavitation bubble for amyloid beta fibril. Sci. Rep. 6, 22015.

Nakajima, K., Toda, H., Yamaguchi, K., So, M., Ikenaka, K., Mochizuki, H., Goto, Y., Ogi, H., 2021b. Half-time heat map reveals ultrasonic effects on morphology and kinetics of amyloidogenic aggregation reaction. ACS Chem. Neurosci. 12, 3456-3466.

Nakamura, A., Kaneko, N., Villemagne, V.L., Kato, T., Doecke, J., Dore, V., Fowler, C., Li, Q.X., Martins, R., Rowe, C., Tomita, T., Matsuzaki, K., Ishii, K., Ishii, K., Arahata, Y., Iwamoto, S., Ito, K., Tanaka, K., Masters, C.L., Yanagisawa, K., 2018. High performance plasma amyloid-beta biomarkers for Alzheimer's disease. Nature 554, 249-254.

Noji, M., Samejima, T., Yamaguchi, K., So, M., Yuzu, K., Chatani, E., Akazawa-Ogawa, Y., Hagihara, Y., Kawata, Y., Ikenaka, K., Mochizuki, H., Kardos, J., Otzen, D.E., Bellotti, V., Buchner, J., Goto, Y., 2021. Breakdown of supersaturation barrier links protein folding to amyloid formation. Commun. Biol. 4, 120.

Noji, M., Sasahara, K., Yamaguchi, K., So, M., Sakurai, K., Kardos, J., Naiki, H., Goto, Y., 2019. Heating during agitation of beta2-microglobulin reveals that supersaturation breakdown is required for amyloid fibril formation at neutral pH. J. Biol. Chem. 294, 15826-15835.

Ohhashi, Y., Kihara, M., Naiki, H., Goto, Y., 2005. Ultrasonication-induced amyloid fibril formation of beta2-microglobulin. J. Biol. Chem. 280, 32843-32848.

Orru, C.D., Groveman, B.R., Hughson, A.G., Zanusso, G., Coulthart, M.B., Caughey, B., 2015. Rapid and sensitive RT-QuIC detection of human Creutzfeldt-Jakob disease using cerebrospinal fluid. MBio. 6.

Paciotti, S., Bellomo, G., Gatticchi, L., Parnetti, L., 2018. Are we ready for detecting alpha-synuclein prone to aggregation in patients? The case of "protein-misfolding cyclic amplification" and "real-time quaking-induced conversion" as diagnostic tools. Front. Neurol. 9, 415.

Parnetti, L., Gaetani, L., Eusebi, P., Paciotti, S., Hansson, O., El-Agnaf, O., Mollenhauer, B., Blennow, K., Calabresi, P., 2019. CSF and blood biomarkers for Parkinson's disease. Lancet Neurol. 18, 573-586.

Saborio, G.P., Permanne, B., Soto, C., 2001. Sensitive detection of pathological prion protein by cyclic amplification of protein misfolding. Nature 411, 810-813.

Sano, K., Atarashi, R., Satoh, K., Ishibashi, D., Nakagaki, T., Iwasaki, Y., Yoshida, M., Murayama, S., Mishima, K., Nishida, N., 2018. Prion-like seeding of misfolded alpha-synuclein in the brains of dementia with Lewy body patients in RT-QUIC. Mol. Neurobiol. 55, 3916-3930.

Sawada, M., Yamaguchi, K., Hirano, M., Noji, M., So, M., Otzen, D., Kawata, Y., Goto, Y., 2020. Amyloid formation of alpha-synuclein based on the solubility- and supersaturation-dependent mechanism. Langmuir 36, 4671-4681.

Sawaya, M.R., Hughes, M.P., Rodriguez, J.A., Riek, R., Eisenberg, D.S., 2021. The expanding amyloid family: Structure, stability, function, and pathogenesis. Cell 184, 4857-4873.

Shahnawaz, M., Mukherjee, A., Pritzkow, S., Mendez, N., Rabadia, P., Liu, X., Hu, B., Schmeichel, A., Singer, W., Wu, G., Tsai, A.L., Shirani, H., Nilsson, K.P.R., Low, P.A., Soto, C., 2020. Discriminating alpha-synuclein strains in Parkinson's disease and multiple system atrophy. Nature 578, 273-277.

So, M., Hall, D., Goto, Y., 2016. Revisiting supersaturation as a factor determining amyloid fibrillation. Curr. Opin. Struct. Biol. 36, 32-39.

So, M., Ishii, A., Hata, Y., Yagi, H., Naiki, H., Goto, Y., 2015. Supersaturation-limited and unlimited phase spaces compete to produce maximal amyloid fibrillation near the critical micelle concentration of sodium dodecyl sulfate. Langmuir 31, 9973-9982.

So, M., Kimura, Y., Yamaguchi, K., Sugiki, T., Fujiwara, T., Aguirre, C., Ikenaka, K., Mochizuki, H., Kawata, Y., Goto, Y., 2021. Polyphenol-solubility alters amyloid fibril formation of alpha-synuclein. Protein Sci. 30, 1701-1713.

So, M., Yagi, H., Sakurai, K., Ogi, H., Naiki, H., Goto, Y., 2011. Ultrasonication-dependent acceleration of amyloid fibril formation. J. Mol. Biol. 412, 568-577.

Soto, C., Saborio, G.P., Anderes, L., 2002. Cyclic amplification of protein misfolding: application to prion-related disorders and beyond. Trends. Neurosci. 25, 390-394.

Stathopulos, P.B., Scholz, G.A., Hwang, Y.M., Rumfeldt, J.A., Lepock, J.R., Meiering, E.M., 2004. Sonication of proteins causes formation of aggregates that resemble amyloid. Protein Sci. 13, 3017-3027.

Tokuda, T., Salem, S.A., Allsop, D., Mizuno, T., Nakagawa, M., Qureshi, M.M., Locascio, J.J., Schlossmacher, M.G., El-Agnaf, O.M., 2006. Decreased alpha-synuclein in cerebrospinal fluid of aged individuals and subjects with Parkinson's disease. Biochem. Biophys. Res. Commun. 349, 162-166.

Umemoto, A., Yagi, H., So, M., Goto, Y., 2014. High-throughput analysis of the ultrasonication-forced amyloid fibrillation reveals the mechanism underlying the large fluctuation in the lag time. J. Biol. Chem. 289, 27290-27299

Vonnegut, K., 1963. Cat's cradle. Dell Publishing, New York.

Wallace, A.F., Hedges, L.O., Fernandez-Martinez, A., Raiteri, P., Gale, J.D., Waychunas, G.A., Whitelam, S., Banfield, J.F., De Yoreo, J.J., 2013. Microscopic evidence for liquid-liquid separation in supersaturated CaCO3 solutions. Science 341, 885-889.

Wetzel, R., 2006. Kinetics and thermodynamics of amyloid fibril assembly. Acc. Chem. Res. 39, 671-679.

Yamaguchi, K., Hasuo, K., So, M., Ikenaka, K., Mochizuki, H., Goto, Y., 2021. Strong acids induce amyloid fibril formation of beta2-microglobulin via an anion-binding mechanism. J. Biol. Chem. 297, 101286.

Yamaguchi, K., Naiki, H., Goto, Y., 2006. Mechanism by which the amyloid-like fibrils of a beta2-microglobulin fragment are induced by fluorine-substituted alcohols. J. Mo.l Biol. 363, 279-288.

Yoshimura, Y., Lin, Y.X., Yagi, H., Lee, Y.H., Kitayama, H., Sakurai, K., So, M., Ogi, H., Naiki, H., Goto, Y., 2012. Distinguishing crystal-like amyloid fibrils and glass-like amorphous aggregates from their kinetics of formation. Proc. Natl. Acad. Sci. U. S. A. 109, 14446-14451.

Yoshimura, Y., Sakurai, K., Lee, Y.H., Ikegami, T., Chatani, E., Naiki, H., Goto, Y., 2010. Direct observation of minimum-sized amyloid fibrils using solution NMR spectroscopy. Protein Sci. 19, 2347-2355.

Yoshimura, Y., So, M., Yagi, H., Goto, Y., 2013. Ultrasonication: an efficient agitation for accelerating the supersaturation-limited amyloid fibrillation of proteins. Jap. J. App. Phys. 52, 01-08.

Table 1. Acceleration of amyloid fibril formation by amplification of seed fibrils or promotion of spontaneous fibril formation

Methods	Major effects	Comments	References
Mechanical agitations			
Ultrasonication	(1)	Similar to PCR, PMCA performs amplification of seed amyloid fibrils by ultrasonication-dependent breakage and elongation of broken seed amyloid fibrils in the presence of monomers.	(Becker et al., 2018; Morales et al., 2012; Saborio et al., 2001; Shahnawaz et al., 2020; Soto et al., 2002)
	(2)	HANABI focuses on the spontaneous amyloid fibril formation. It is also useful for amplifying seed amyloid fibrils by the same mechanism as PMCA or RT-QuIC. Compared with shaking/stirring, ultrasonication suppresses the formation of amorphous aggregates.	(Kakuda et al., 2019; Nakajima et al., 2021a; Umemoto et al., 2014; Yoshimura et al., 2012; Yoshimura et al., 2013)
Shaking or stirring	(1)	RT-QuIC amplifies seed amyloid fibrils by shaking- or stirring-dependent breakage and elongation mechanism.	(Atarashi et al., 2011; Fairfoul et al., 2016; Orru et al., 2015; Sano et al., 2018)
	(2)	Shaking or stirring is also useful for acceleration of spontaneous amyloid fibril formation	(Giehm and Otzen, 2010; Kad et al., 2003; Yoshimura et al., 2012)
Additives and solvent conditions			
Salts or acids	(2)	Various salts or acids accelerate amyloid fibril formation by the anion-binding or salting-out mechanism. Too high concentrations of these cosolvents produce amorphous aggregates, thus preventing amyloid fibril formation.	(Goto et al., 2018; Yamaguchi et al., 2021)
Detergents, alcohols or other cosolvents	(2)	Detergents or alcohols accelerate amyloid fibril formation by promoting hydrophobic interactions of amyloidogenic proteins. Too high concentrations of these cosolvents dissolve amyloidogenic proteins, thus preventing amyloid formation. The effects of other cosolvents (e.g. polyphenols) can be explained by a similar mechanism.	(Muta et al., 2014; Sawada et al., 2020; So et al., 2015; So et al., 2021; Yamaguchi et al., 2006)

Beads or nanoparticles	(2)	A tiny amount of particles may accelerate amyloid fibril formation by concentrating amyloidogenic proteins. However, too high concentrations may prevent amyloid fibril formation by forming amorphous aggregates	(Abdolvahabi et al., 2017; Linse et al., 2007)
High temperature	(2)	Because hydrophobic interactions strengthen upon increasing temperature, higher temperatures (at 40-80 °C) may accelerate amyloid fibril formation more than previously assumed.	(Adachi et al., 2015; Noji et al., 2021; Noji et al., 2019)
Isoelectric point (pI)	(2)	A balance of electrostatic and hydrophobic interactions makes pI without salts to be an optimal condition for amyloid fibril formation of aSN.	(Furukawa et al., 2020)

Figure legends

Fig. 1. Protein and salt concentration-dependent phase diagram common to native crystals and aggregates of denatured proteins. Regions 1, 2, 3, and 4 represent under saturation, metastable, labile, and amorphous regions, respectively. Crystallization and amyloid fibril formation occur from regions 2 and 3. The figure was modified from So et al. (So et al., 2016) with permission.

Fig. 2. Assay of amyloid fibrils using a combination of ultrasonication and a microplate reader. (A) Illustration of the experimental procedures. The microplate was set on a water bath-type ultrasonicator at the center for maximal ultrasonication. Pulses were applied to the microplate from three directions. The power and output of the sonication were set to 17-20 kHz and 350 watts, respectively, and the temperature was maintained at 37 ºC. The formation of fibrils was monitored by ThT fluorescence with a microplate reader with excitation and emission wavelengths of 450 and 490 nm, respectively. t_{lag} was defined by the time at which ThT fluorescence reached five-fold of the standard deviation of the mean intensity at time 0. The distinct kinetic data are represented by the gradient of colors: red for the fastest to blue for the slowest. (B) Time-course of fibril formation in 96 wells monitored using ThT fluorescence. Lines of different colors represent the kinetics in different wells as defined by the color scale bar. (C) Control experiments monitoring the formation of fibrils by shaking (○) or under quiescent conditions (Δ). For each condition, 10 wells were used and the results of three wells are presented. Fibrils formed in only one of 10 wells shaken. (D) AFM images of fibrils produced by ultrasonication for 1 min every 10 min (i) or 10 min every 15 min (ii) and by seeding reaction without ultrasonication (iii). The

white scale bar represents 1 μm. The figure was reproduced from So et al. (So et al., 2016) with permission.

Fig. 3. Overview (A) and schematic illustration (B) of HANABI. The figure was reproduced from Umemoto et al. (Umemoto et al., 2014) with permission.

Fig. 4. Performance of HANABI with β2m. A microplate with 96 wells containing 0.3 mg/ml β2m in 100 mM NaCl and 5 μM ThT at pH 2.5 was ultrasonicated by cycles of 1-min ultrasonication and 9-min quiescence with (D-F) and without (A-C) plate movements at 37 °C. Kinetics (A, D) monitored by ThT fluorescence at 480 nm and schematic representations of the plates (B, E) are shown by different colors according to the lag time, as defined by the color scale bar in panel D. *(*C, F*)* Representative TEM images of fibrils obtained after 12-h ultrasonication. (G) Histograms of the lag time with (red) and without (blue) plate movements. (H, I) The average lag times with standard deviations (H) and coefficients of variation (I). The figure was modified from Umemoto et al. (Umemoto et al., 2014) with permission.

Fig. 5. Monitoring the crystallization of lysozyme with HANABI. (A, B) Crystallization with (B) and without (A) 5-min ultrasonication. (C) Crystallization with 5-min ultrasonication followed by quiescence. (D) Crystallization with 5-min ultrasonication followed by 30-min quiescence, 1-min ultrasonication, and quiescence. (E) Crystallization in various wells with 5-min ultrasonication

followed by quiescence for 50 h. Sizes of images were 3 x 4 mm. The figure was modified from Umemoto et al. (Umemoto et al., 2014) with permission.

Fig. 6. Overview of the HANABI-2000 system. (A) 3D schematic illustration of the optimized sonoreactor for the amyloid-fibril assays, HANABI-2000. The dimensions of the device are 500 × 550 × 550 mm^3. (B) Block chart of the control units of HANABI-2000. The figure was reproduced from Nakajima et al. with permission (Nakajima et al., 2021a).

Fig. 7. Aggregation acceleration model focused on cavitation-bubble dynamics. (A) Ultrasonic waves (i.e., 20–300 kHz) develop compression and rarefaction while transmitting through the medium. Bubbles are generated in solution by negative pressure of ultrasonic waves. (B) Bubbles grow in the negative-pressure phase, during which time Aβ monomers (yellow hairpin-shaped bars) are absorbed on bubble surfaces by hydrophobic interactions. (C) Bubbles collapse under positive pressure of ultrasonic waves, leading to local condensation of Aβ monomers and a temperature increase in and near the bubbles. The figure was reproduced from Nakajima et al. with permission (Nakajima et al., 2016).

Fig. 8. Half-time (t_{half}) heat maps of aggregation reactions. (A) Under quiescence, (B) under shaking, and (C) under ultrasonication. The yellow dots denote the solubility of acidic β2m monomer at each salt concentration determined by ultracentrifugation and the ELISA assay**.** The dotted lines in panels B and C indicate the phase boundaries under quiescence, which are varied

under agitation. The figure is reproduced from Nakajima et al. (Nakajima et al., 2021b) with permission.

Goto et al., Fig. 1

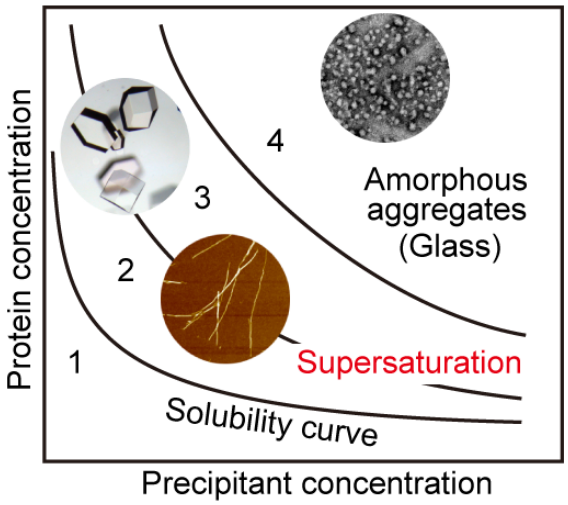

Goto et al., Fig. 2

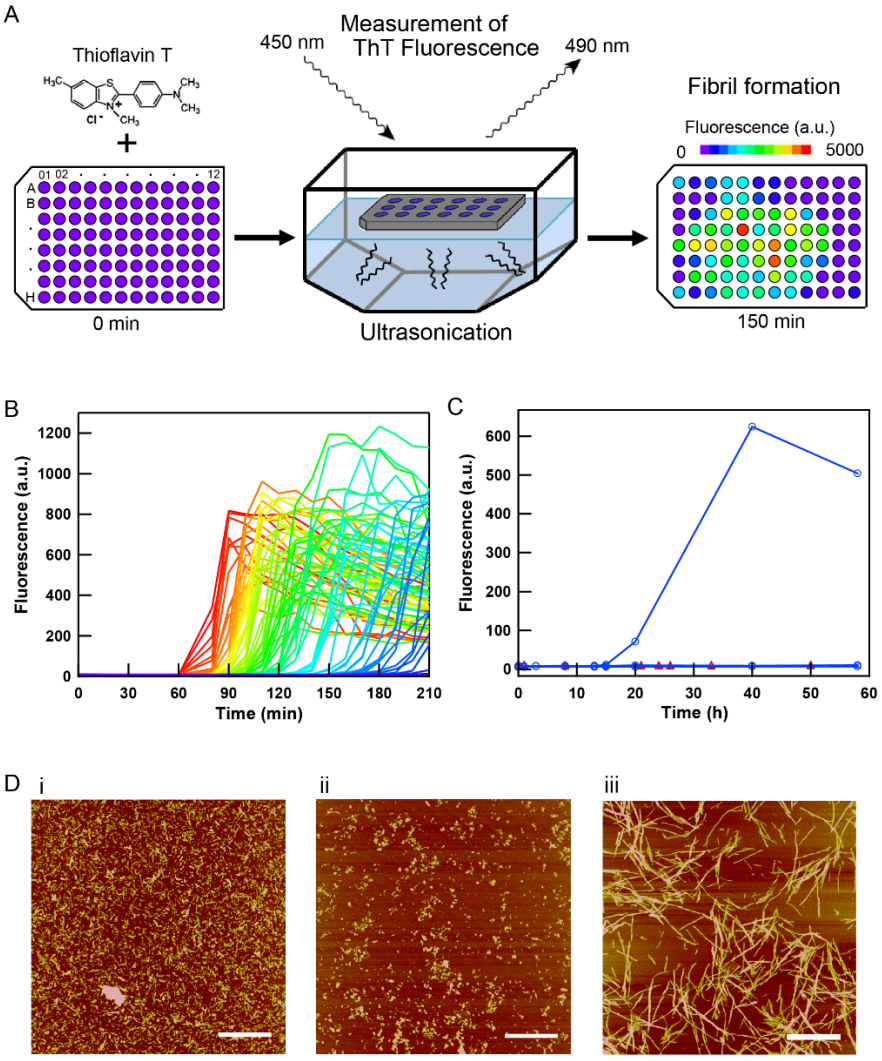

Goto et al., Fig. 3

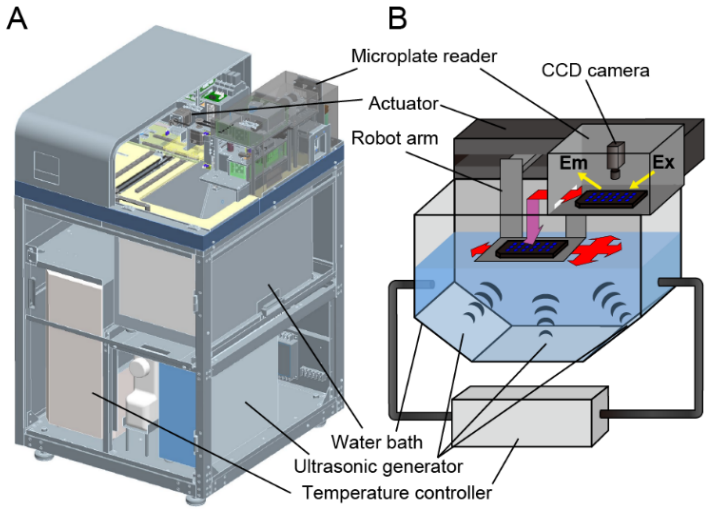

Goto et al., Fig. 4

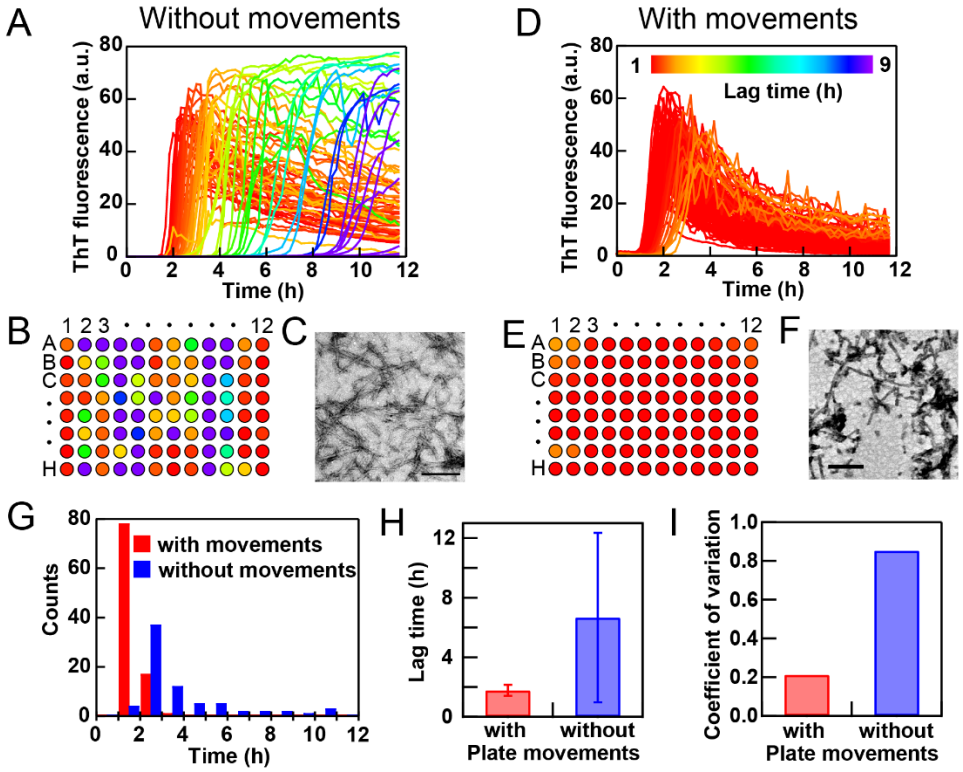

Goto et al., Fig. 5

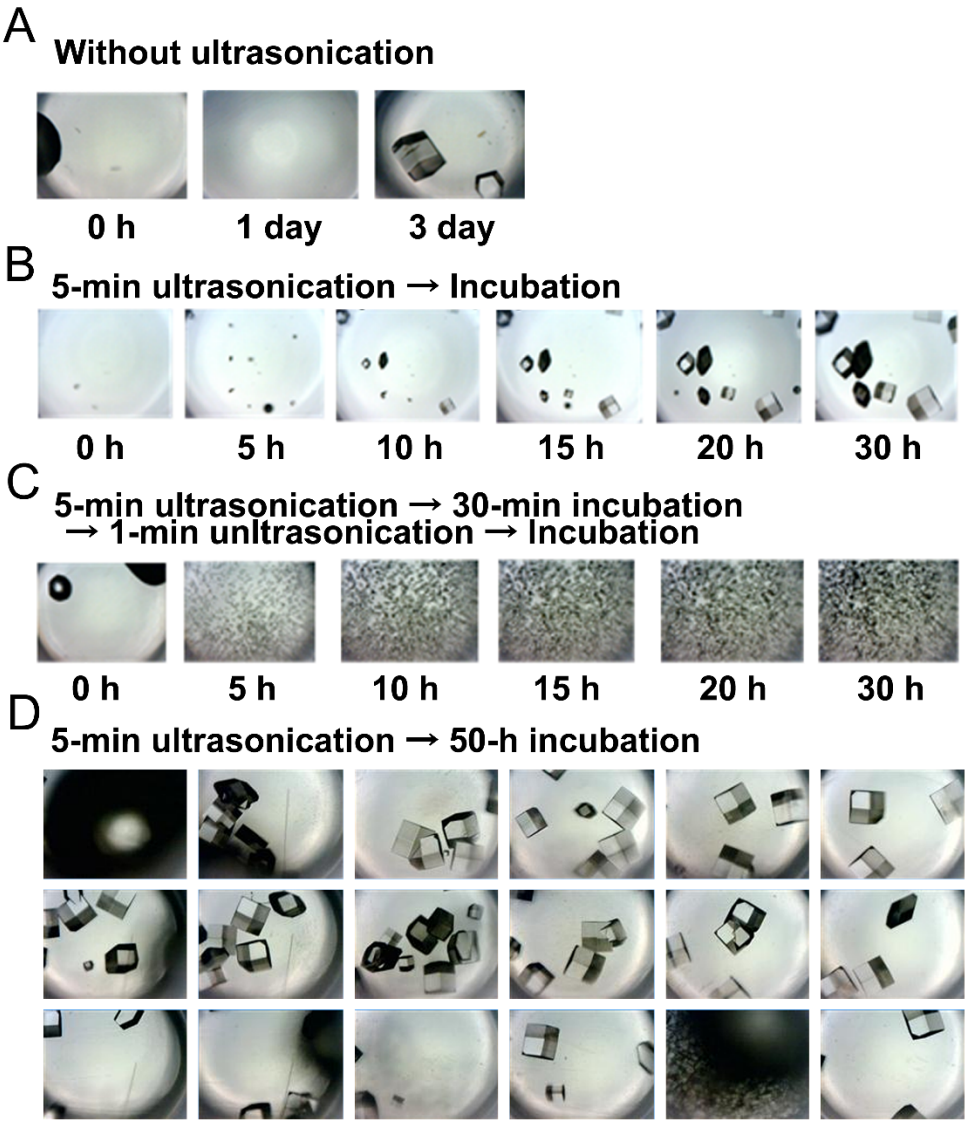

Goto et al., Fig. 6

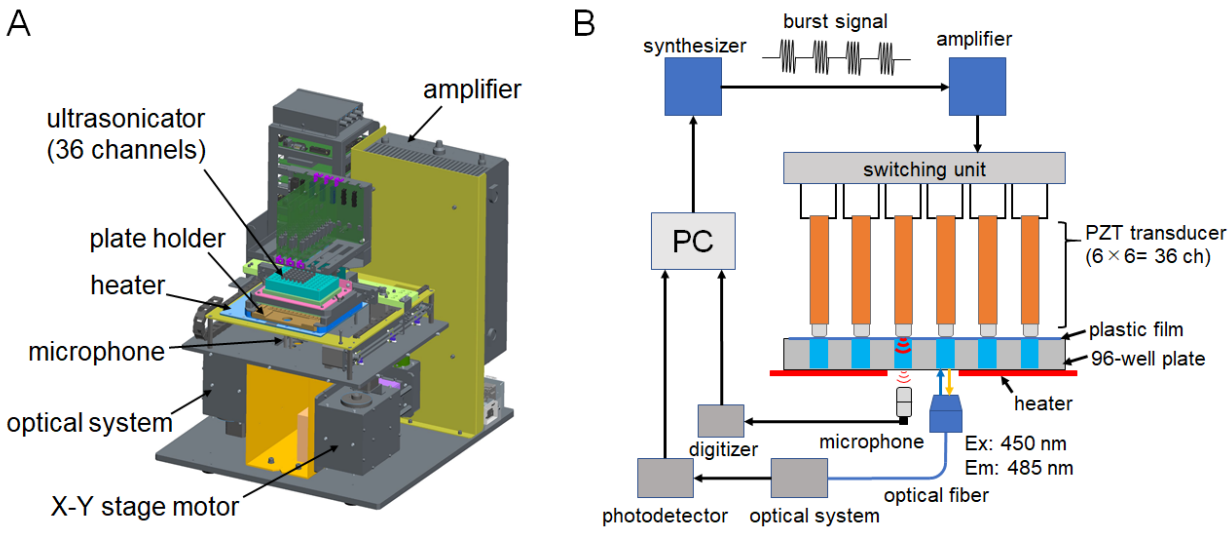

Goto et al., Fig. 7

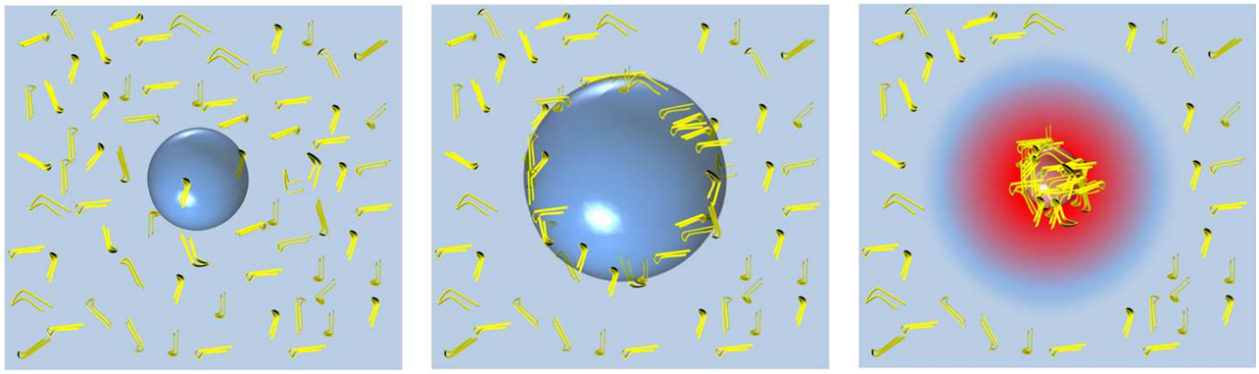

Goto et al., Fig. 8